Polym. Korea, Vol. 48, No. 6, pp. 639-648 (2024)
https://doi.org/10.7317/pk.2024.48.6.639

ISSN 0379-153X(Print)
ISSN 2234-8077(Online)

고성능 양쪽성 이온 하이드로겔 고분자 전해질 기반 수계 아연 이온 배터리: 뛰어난 이온 전도도와 안정성을 갖춘 전해질

한다야니 푸지 레스타리[#] · 이예지[#] · 최우혁[†]
인하대학교 고분자공학과 및 고분자환경융합공학전공
(2024년 6월 4일 접수, 2024년 6월 13일 수정, 2024년 8월 16일 채택)

High-Performance Zwitterionic Hydrogel Polymer Electrolytes for Aqueous Zinc-Ion Batteries: Superior Ionic Conductivity and Stability

Puji Lestari Handayani[#], Ye Ji Lee[#], and U Hyeok Choi[†]
Department of Polymer Science and Engineering and Program in Environmental and Polymer Engineering, Inha University, Incheon 22212, Korea
(Received June 4, 2024; Revised June 13, 2024; Accepted August 16, 2024)

초록: 본 연구에서는 아연이온과 물 분자간 강한 상호작용으로 인한 덴드라이트 및 음극 부식 문제를 해결하기 위해 양쪽성 이온이 포함된 하이드로겔 고분자 전해질을 제작하였다. 이를 위해 acryl amide(AM)와 양쪽성 이온인 vinyl imidazole propane sulfonate(VIPS)를 단량체로, vinyl silica nanoparticle(VSN)을 가교제로, 그리고 $ZnSO_4$와 LiCl을 전해질 염으로 하여 UV 가교를 통해 고상형 전해질을 중합하였다. 하이드로겔 고분자 전해질[P(AM-*co*-IPS)-$ZnSO_4$/LiCl]은 높은 상온 이온 전도도(σ_{DC} = 3.5 × 10^{-2} S/cm)를 나타내었다. 또한 양쪽성 이온과 LiCl의 첨가로 아연의 용매화 구조가 안정화되어 낮은 어는점(T_m = -33.3 ℃) 뿐만 아니라, 수소 발생 전위(HER, -52 mV) 및 부식 전류(1840 μA) 또한 감소함을 확인했다. 결과적으로 400시간 이상 안정적으로 구동하는 셀을 제작하여 추후 수계아연전지로의 적용이 기대된다.

Abstract: We developed hydrogel polymer electrolytes for use in aqueous zinc-ion batteries. Aqueous zinc batteries face challenges related to dendrite formation and corrosion at the zinc metal anode, primarily stemming from the strong interaction between zinc ions and water molecules. To address this, we designed hydrogel polymer electrolytes, composed of acrylamide (AM) and zwitterion, such as vinyl imidazole propane sulfonate (VIPS), as monomers, vinyl silica nanoparticles (VSN) as cross-linkers, and zinc sulfate ($ZnSO_4$) and lithium chloride (LiCl) as salts, through UV polymerization. The resulting hydrogel polymer electrolyte [P(AM-*co*-IPS)-$ZnSO_4$/LiCl] exhibited high ionic conductivity (σ_{DC} = 3.5 × 10^{-2} S/cm) and remarkable flexibility (elongation at break = 321%) at 298 K. The addition of zwitterion and lithium chloride stabilized the solvation structure of zinc salts, leading to a reduction in melting points (from -25.4 to -33.3 ℃), hydrogen evolution potential (HER, -52 mV), and corrosion current (1840 μA). The zinc symmetric cell demonstrated that our electrolyte not only showed a high zinc ion transference number ($t_{Zn^{2+}}$ = 0.7), but also maintained stable cell operation for over 400 hours, due to the effective ion transport channels facilitated by zwitterions.

Keywords: aqueous zinc-ion battery, zwitterion, hydrogel polymer electrolyte, ionic conductivity.

Introduction

In the modern world, energy storage systems are considered pivotal elements for sustainable energy supply and power distribution.[1-4] In this context, flexible aqueous zinc-ion batteries (AZIB) have garnered significant attention as promising candidates for next-generation batteries.[5-7] Aqueous zinc-ion batteries offer several advantages such as excellent safety, low zinc cost, environmental friendliness, and high theoretical capacity of Zn (820 mAh/g). This makes them integral to future energy storage systems including portable power devices and renewable energy systems.[8] However, AZIB still suffers from side reactions, such as hydrogen evolution reaction (HER) and corrosion in the zinc anode during charge and discharge cycles, as well as issues related to freezing below subzero temperatures caused by the presence of water.[9-12] These disadvantages restrict

[#]P. L. H. and Y. J. L. contributed equally to this work
[†]To whom correspondence should be addressed.
uhyeok@inha.ac.kr, ORCID 0000-0002-0048-9550

commercialization by reducing the efficiency of the system.

To address these issues, hydrogel polymer electrolytes have garnered attention as a potential solution. They consist of a water-absorbing polymer network matrix that not only enhances mechanical stability without sacrificing ionic conductivity, but also prevents leakage of liquid electrolyte components.[13,14] Traditional hydrogel electrolytes have successfully formed a polymer matrix and enhanced properties using water as a solvent, without compromising ion conductivity. However, achieving significant improvement in electrochemical performance has not been very successful.[15]

In this study, we designed a zwitterion-based hydrogel polymer electrolyte [P(AM-*co*-IPS)-$ZnSO_4$/LiCl] (Figure 1). The zwitterionic groups of imidazole propane sulfonate (IPS) could promote the ion migration channel formation and ion dissociation of electrolyte salts ($ZnSO_4$ or LiCl) and suppress HER by forming a solvation structure. Zwitterionic polymer hydrogel electrolytes, in particular, exhibit remarkable characteristics due to their unique molecular structure that contains both cationic and anionic functional groups.[16-18] This distinctive feature allows them to improve ion mobility through electrostatic interaction with electrolyte ions by forming ion migration channels. Zwitterions, together with the solvation structure formed with water molecules, effectively inhibit undesirable side reactions such as the HER and dendrite formation. These advantages of zwitterion-based hydrogel polymer electrolytes not only enhance the overall performance of zinc-ion batteries, but also significantly contribute to their safety and longevity.[14,19,20] The vinyl silica nanoparticles (VSNs) act as chemical cross-linkers, improving the mechanical properties.[21] Lithium chloride (LiCl) serves as an anti-freezing component, and the Cl^- anion forms a solvation structure with Zn^{2+} cation to help suppress water activity.[22-24] Consequently, our hydrogel polymer electrolytes showed a high zinc ion transference number ($t_{Zn^{2+}}$ = 0.7), reduced corrosion potential, and stable cycle performance over 400 hours in zinc stripping/plating tests. To optimize this system, the properties were systematically analyzed through various tests and analysis methods.

Experimental

Materials. Acryl amide (AM), zinc sulfate solution (2 M $ZnSO_4$), lithium chloride (LiCl), N,N′-methylenebisacrylamide (MBA), and 2-hydroxy-4′-(2-hydroxyethoxy)-2-methylpropiophenone (referred to as Irgacure 2959) were purchased from Sigma Aldrich, Korea. Triethoxyvinylsilane, 1-vinylimidazole, 1,3-propane sulfonate, zinc foil, and stainless steel foil were purchased from MTI, Korea. Diethyl ether (99.5%) and acetone (99%) were obtained from Samchun Pure Chemical, Korea. Deionized (DI) water was used for all experiments.

Synthesis of Vinyl Silica Nanoparticle (VSN), Vinyl Imidazole Propane Sulfonate (VIPS), and Hydrogel Polymer Electrolyte ([P(AM-*co*-IPS)-$ZnSO_4$/LiCl]. *VSN*: As described in our previous report,[21] the VSN cross-linker was prepared by dispersing triethoxyvinylsilane (0.95 g) in deionized water (7.5 mL) and stirring the mixture for 12 h at room temperature. Subsequently, the homogeneous solution was stirred for an additional 2 h at 60 ℃, resulting in a sol-gel reaction that produced silica nanopar-

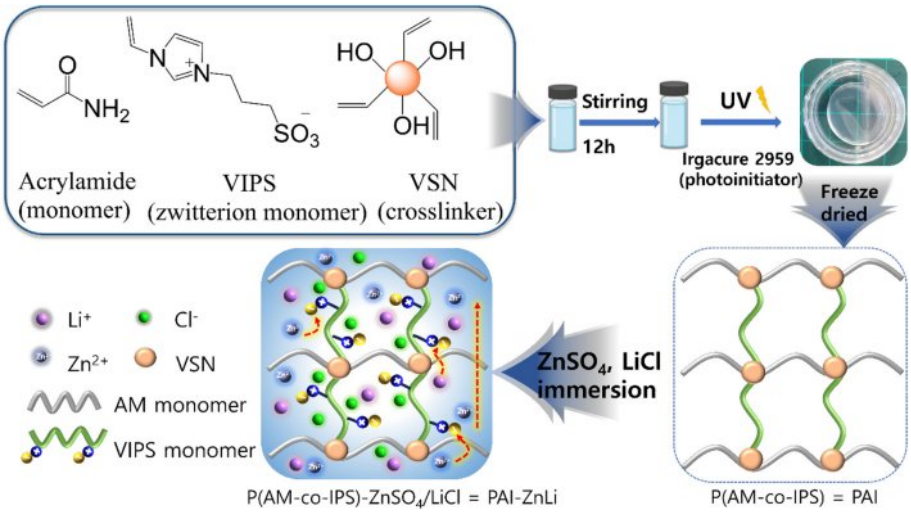

Figure 1. Synthesis schematic of hydrogels, P(AM-*co*-IPS) = PAI, including the photo image, and hydrogel polymer electrolytes, P(AM-*co*-IPS)-$ZnSO_4$/LiCl = PAI-ZnLi.

ticles dispersed in water.

VIPS: Vinyl-functionalized zwitterion was synthesized following a previous report with modifications.[25] 1-Vinylimidazole (12.6 g) was added to a 2-neck flask containing acetone (160 mL) during stirring. Subsequently, 1,3-propane sulfonate (16.4 g) was slowly introduced to the solution at 0 ℃ under a nitrogen (N_2) atmosphere. The solution was stirred at room temperature for 5 days. The resulting product was washed with diethyl ether and dried under vacuum (OV4-65, Vacuum Oven, JEIO TECH, Korea) at room temperature for 12 h, yielding a white powder.

P(AM-co-IPS) and P(AM-co-IPS)-ZnSO$_4$/LiCl: P(AM-*co*-IPS) (referred to as PAI) was achieved through a one-pot UV polymerization involving acrylamide (AM, 0.27 g) and vinyl imidazole propane sulfonate (VIPS, 0.105 g) monomers, where vinyl silica nanoparticles (0.075 g) and Irgacure 2959 (0.008 g) were employed as cross-linkers and photo-initiator, respectively. The four components were added to deionized (DI) water (1.05 g) and stirred at room temperature for 12 h. The resulting homogeneous solution was poured into a home-made mold and exposed to UV light (UV Lamps, VL-6.LC, Vilber Lourmat, Germany) for 2 h to achieve complete polymerization. For the preparation of the salts ($ZnSO_4$ and LiCl)-containing hydrogel polymer electrolyte [P(AM-*co*-IPS)-$ZnSO_4$/LiCl, referred to as PAI-ZnLi], the obtained hydrogel PAI was initially freeze-dried (Hypercool, HC3110, Hanil Scientific Inc., Korea) at -109 ℃ for 48 h. Subsequently, the dried PAI hydrogel was immersed in an aqueous solution containing 2 M $ZnSO_4$ and 4 M LiCl until it reached an equilibrium state. This resulted in the formation of transparent, flexible cross-linked hydrogel polymer electrolytes (PAI-ZnLi). For the comparison, hydrogel polymer electrolytes containing only Zn salt (10 mL) (PAI-Zn) were prepared using the same method but without LiCl salt. The prepared hydrogel polymer electrolytes were denoted as PAIx-ZnLi, where x = 0, 5, and 7, representing the weight fraction of the zwitterion VIPS.

Characterization. Fourier transform infrared spectroscopy (FTIR, Shimadzu, IRAffinity-1S, Shimadzu Corporation, Japan) analysis was conducted with a diamond attenuated total reflectance (ATR) cell. The spectra were recorded in the range of 500 to 4000 cm^{-1} to analyze the chemical structures of our samples. Density functional theory (DFT) calculations were performed using the Gaussian 05 Software packaged using the 6-31G B3LYP function to find optimized structures and binding energies between various components (such as VIPS, H_2O, $ZnSO_4$, and LiCl) within the hydrogel polymer electrolyte system. Differential scanning calorimetry (DSC) (TA Instrument, DSC 25, USA) was used to investigate the thermal properties of hydrogel polymer electrolytes. The heating and cooling rate was 10 ℃/min, and the temperature range was between -60 to 60 ℃ under an N_2 atmosphere. The ionic conductivity (σ_{DC}) was measured with temperature-controlled electrochemical impedance spectroscopy (TC-EIS) measurement (Biologic Potensiostat, VSP-300, France), in a temperature range of 30 to -30 ℃. The sample was cut into a round shape and sandwiched between two aluminum electrodes. The ionic conductivity was measured in the frequency from 10^6 to 10^{-1} Hz, with a potential amplitude of 141.4 mV, and calculated by the following Eq. (1)[3]:

$$\sigma_{DC} = \frac{l}{RA} \tag{1}$$

where l, R, and A are the sample thickness, resistance, and the area of the top electrode, respectively. A universal testing machine (UTM, Instron, 5569, USA) was used to test the mechanical properties of hydrogel polymer electrolytes, with 20 mm/min velocity and using a 2.5 N load cell. For the Swagelok cell tests (Biologic Potensiostat, VSP-300, France), stainless steel (SS)||Zn asymmetric cell and Zn||Zn symmetric cell were assembled with hydrogel polymer electrolytes. Linear sweep voltammetry (LSV) and cyclic voltammetry (CV) tests were conducted using SS||Zn cell at a scan rate of 0.1 mV/s. The Tafel test using Zn||Zn cell was performed at 0.1 mV/s. The chronoamperometry test to calculate the transference number of Zn ions ($t_{Zn^{2+}}$) was performed using Zn||Zn cell under polarized voltage at 10 mV for 3600 s. The $t_{Zn^{2+}}$ value was calculated by the following Eq. (2):

$$t_{Zn^{2+}} = \frac{I_S(\Delta V - I_0 R_0)}{I_0(\Delta V - I_S R_S)} \tag{2}$$

where I_0 and R_0 are the initial current and resistance before polarization, respectively, I_S and R_S are the steady-state current and resistance after polarization, respectively, and ΔV is the polarization voltage. For the coin cell tests, the Zn||Zn symmetric cell was assembled with hydrogel polymer electrolytes. The zinc stripping/plating test was carried out using a coin cell at a current density of 0.1 mA/cm^2.

Results and Discussion

Synthesis of Hydrogel [P(AM-*co*-IPS) = PAI] and Its Polymer Electrolyte [P(AM-*co*-IPS)-ZnSO$_4$/LiCl = PAI-ZnLi]. Zwitterionic hydrogels P(AM-*co*-IPS) were prepared through one-pot UV polymerization using 2-hydroxy-4′-(2-hydroxyethoxy)-2-methylpropiophenone (Irgacure 2959) as a photoinitiator, resulting in a transparent

hydrogel as displayed in Figure 1. The VIPS zwitterion was introduced to enhance ion dissociation, thus facilitating ion transport for a higher transference number and increased ionic conductivity. First, to prepare the PAI hydrogel, the AM hydrophilic and VIPS zwitterionic monomers were cross-linked with VSN, which serves as cross-linking points and transfers stress to strengthen the hydrogel network structure under any stress or mechanical deformation. VSNs with size < 50 nm were prepared by facile sol-gel reaction, as described in our previous report.[26]

Then, for the synthesis of its electrolyte (PAI-ZnLi), the PAI was freeze-dried for 48 hours to remove water and subsequently soaked in salt-containing aqueous electrolytes, consisting of 2 M $ZnSO_4$ and 4 M LiCl. The employment of highly concentrated cooperative solvents was beneficial in breaking the hydrogen bonds between water molecules, which lowered the freezing point of the hydrogel.[27]

FTIR confirmed the successful synthesis of VIPS and VSN with the appearance of vinyl groups peak at ~960 and 1650 cm^{-1}, as shown in Figure 2(a).[25,28] In addition, the successful polymerization of PAIx-ZnLi was revealed by the absence of the characteristic C=C peak observed at 960 cm^{-1} after the UV cross-linking process (Figure 2(b)).[29] Unlike PAI0-ZnLi, the zwitterion-containing PAI7-ZnLi exhibits an additional characteristic peak at 1040 cm^{-1}, attributed to the -SO_3^- group from the zwitterion IPS.[30] Within the IPS chains, the positively charged group (imidazolium cation) and the negatively charged group (sulfonate anion) are inclined to interact with free cations (Zn^{2+}) or anions (SO_4^{2-}), presumably forming ion migration channels that facilitate ion transport through electrostatic forces.[14,31-33] Furthermore, the hydrophilic IPS chains can form ion-dipole interactions with H_2O molecules, endowing PAI-ZnLi with the capability to suppress H_2O activity.[31] This inhibition effectively restraints the water-induced hydrogen evolution reaction (HER) and corrosion, which will be discussed in a later section.

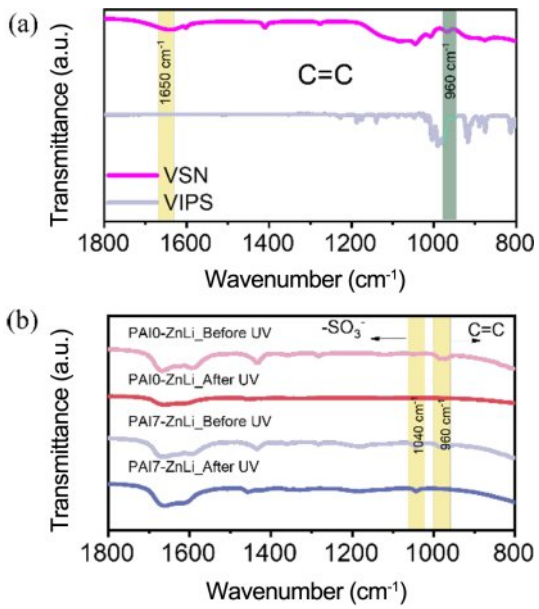

Figure 2. FTIR characterization of (a) VSN and VIPS; (b) PAIx-ZnLi (x = 0 and 7) hydrogel polymer electrolytes before and after the UV curing process.

Mechanical Properties of Hydrogel Polymer Electrolytes, PAIx-ZnLi. The mechanical properties of hydrogel polymer electrolytes are crucial factors in preventing fracture of wearable devices during regular activities. Tensile stress-strain curves were employed to evaluate these mechanical properties of hydrogel polymer electrolytes (Figure 3(a)). In PAI7-ZnLi, the presence of vinyl silica nanoparticles (VSNs) serving as covalent cross-linkers leads to the creation of a polymer network structure with excellent mechanical properties, allowing the resultant hydrogel electrolytes to possess high stretchability. Additionally, VSNs act as stress buffers, enabling energy dissipation and stress transfer.[34] Moreover, the existence of LiCl in the cooperative solvent weakens the hydrogen bonding of the polymer chain, thus improving its mobility.[27] Consequently, for the VSN cross-linker-based PAI7-ZnLi-VSN, the tensile strength increased from 45 to 56 kPa, and the elongation at break significantly improved from 87 to 321%, when compared to hydrogel electrolytes (PAI7-ZnLi-MBA) using the traditional cross-linker (MBA), as shown in Figure 3(a). Furthermore, the PAI7-ZnLi-SN electrolyte exhibits excellent stretchability and flexibility, as demonstrated in Figure 3(b). It is capable of stretch-

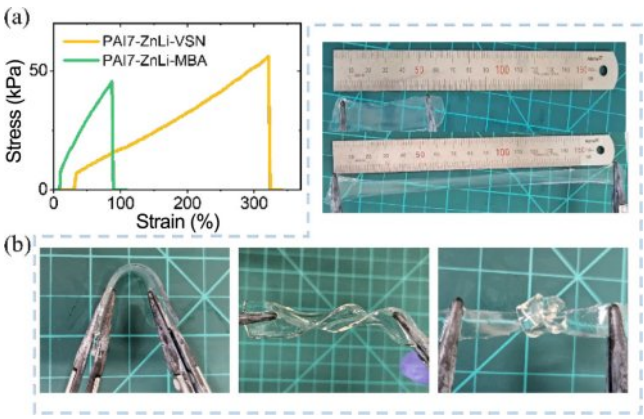

Figure 3. (a) Tensile stress-strain curves of hydrogel polymer electrolytes synthesized by different crosslinking agents (VSN *vs.* MBA); (b) Photographs showing flexible PAI7-ZnLi hydrogel electrolyte under stretching, bending, rolling, and knotting states.

ing, twisting, bending, and knotting, making it suitable for flexible wearable devices.

Water Structure Analysis Using DFT and FTIR. In aqueous zinc electrolytes, zinc metal cations are solvated by dipolar water molecules (H_2O), forming a solvation shell structure [$(Zn(H_2O)_6)^{2+}$].[10] Electron transfer occurs from H_2O to Zn^{2+} cations via the Zn-OH_2 bond, which is facilitated by the strong interaction between cations and water.[10] This results in the weakening of the O-H bond in water, potentially leading to the deprotonation of H_2O. The deprotonation can give rise to the formation of deprotonated species such as $Zn(OH)_2$ or ZnO.[10,13,25,35] Consequently, the cation-water interaction plays a critical role in the HER and also promotes dendrite formation on the anode. The effect of this hydrate structure on HER suggests that the weak interactions between Zn^{2+} cation and water can suppress HER.

It is reported that the Cl^- anions exhibit strong coordination ability with Zn^{2+} cation, allowing them to replace water molecules within the solvation shell structure.[10,31] Moreover, the sulfonate groups in the zwitterion IPS are hydrophilic and zincophilic with high electron density, weakening the hydrogen bonds of water-water, but strengthening the O-H bonds of water.[36] This enhances the electrochemical stability and suppresses HER. For this reason, we choose the lithium chloride salt (LiCl) and IPS monomeric zwitterion to reconstruct the solvation structure, presumably transforming it from $(Zn(H_2O)_6)^{2+}$ to $ZnCl_4^{2-}$ or VIPS-$(Zn(H_2O)_5)^{2+}$. These new solvation structures would suppress HER by releasing bound water molecules, as a result of strong cation-water interaction, into free water molecules.[10] To verify this assumption, the density functional theory (DFT) calculations were employed to determine the binding energies between ions and molecules. Figure 4a shows the optimal configuration of Zn-$(H_2O)_6^{2+}$, Zn-Cl_4^{2-}, and VIPS-Zn^{2+}. In Figure 4b, it is revealed that the binding energy between VIPS and Zn^{2+} (*i.e.*, VIPS-Zn^{2+}) is -445.33 kcal/mol, which is more negative than that between H_2O and Zn^{2+} (-108.8 kcal/mol). The more negative binding energy suggests that the solvation structure of VIPS-$(Zn(H_2O)_5)^{2+}$ with -505.22 kcal/mol is more favorable than one of Zn-$(H_2O)_6)^{2+}$ with -431.38 kcal/mol. Additionally, if there are sufficient Li^+ cations and Cl^- anions, not only $ZnCl_4^{2-}$ solvation structure with a binding energy of -656.2 kcal/mol can be formed, but also Li^+ cations would coordinate with water molecules, forming Li-$(H_2O)_4^+$. To further investigate the bound water structures, the deconvolution of the -OH peak observed in the 4000-2500 cm^{-1} was performed using the FTIR spectra (Figure 4(c) and 4(d)). The OH water peak was categorized into two types, which are free water peak observed at 3210 cm^{-1} and bound water peak observed at 3420 cm^{-1}.[37] In Figure 4(d), the introduction of IPS led to a pronounced free water peak (blue color) and a relatively weaker bound water peak (red color), in contrast to the IPS-free hydrogel electrolyte (Figure 4(c)). As a result, in the quantitative analysis of the relative peak area frac-

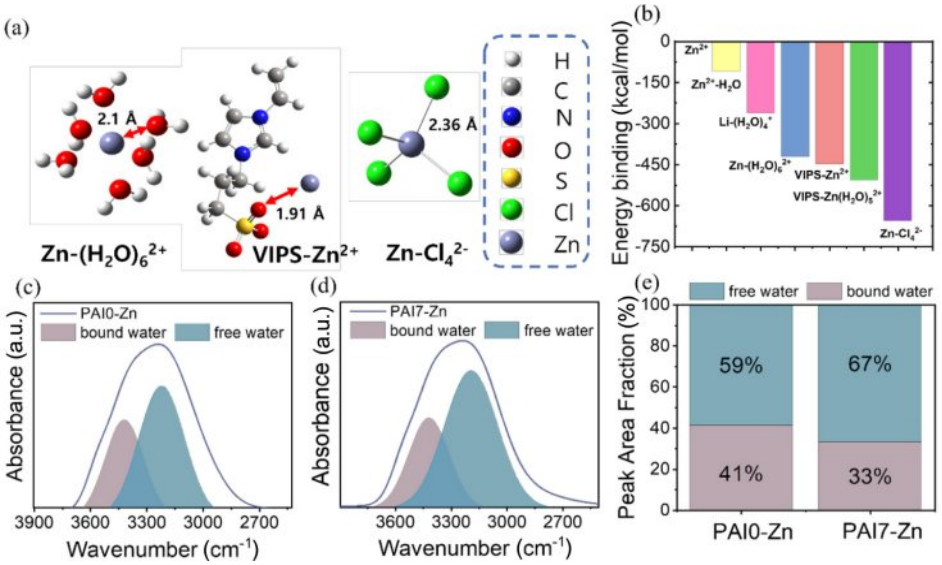

Figure 4. (a, b) DFT calculations showing (a) optimized configurations of Zn-$(H_2O)_6^{2+}$, Zn-Cl_4^{2-}, and VIPS-Zn^{2+} and (b) the binding energies between various components (such as VIPS, H_2O, $ZnSO_4$, and LiCl) within hydrogel electrolyte system; (c, d) Deconvolution of FTIR peaks corresponding to bound water peaks at 3420 cm^{-1} and free water peaks at 3210 cm^{-1} for (c) PAI0-Zn; (d) PAI7-Zn; (e) Area fraction of the deconvoluted peaks corresponding to bound water and free water.

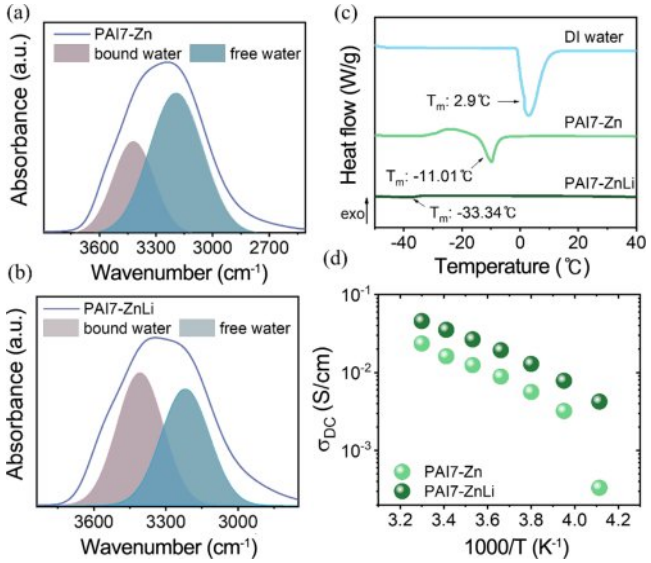

Figure 5. (a, b) Deconvolution of FTIR peaks corresponding to bound water peaks at 3420 cm^{-1} and free water peaks at 3210 cm^{-1}; (a) PAI7-Zn; (b) PAI7-ZnLi; (c) DSC results of DI water, PAI7-Zn, and PAI7-ZnLi; (d) EIS temperature controller analysis of PAI7-Zn and PAI7-ZnLi hydrogel polymer electrolytes.

tions (Figure 4(e)), the fraction of free water increased from 59% to 67%. This confirms that the increase in free water content is a direct result of the changes in the solvation structure induced by the VIPS zwitterion.

Thermal and Ionic Conducting Properties. To investigate the impact of lithium chloride (LiCl) on the freezing point, the deconvolution of the -OH peak observed in the 4000-2500 cm^{-1} was performed using the FTIR spectra with and without LiCl. In the absence of LiCl (Figure 5(a)), a prominent peak of free water was observed, whereas in the presence of LiCl (Figure 5(b)), the peak of bound water significantly increased.[38] This implies a strong binding of lithium with water, and it is known that lithium-bound water lowers the freezing point.[38,39] Moreover, in the DSC heating cycle (from -55 to 30 ℃), a comparison between PAI7-Zn and PAI7-ZnLi revealed a decrease in the freezing point from T_m = -11.01 to -33.34 ℃, respectively, and their T_m values were much lower that of DI water (T_m = 2.9 ℃) (Figure 5(c)). Additionally, Figure 5d shows the temperature dependence of ionic conductivity σ_{DC}(T) and demonstrates that for PAI7-Zn, the ion conductivity sharply decreased by approximately one order of magnitude at around -30 ℃. In contrast, PAI7-ZnLi exhibited the absence of discontinuities in σ_{DC}(T), suggesting that even at -30 ℃, water does not freeze, allowing ions to transport freely, consistent with the observation from DSC.

Electrochemical Performance. In aqueous zinc-ion batteries, issues related to side reactions and irreversibility at the anode due to water activity, remain to be addressed. The strong interaction between Zn^{2+} cations and water molecules leads to parasitic reactions, such as the production of by-products and hydrogen gas, driven by highly activated water molecules.[9,10,23,40–42] Hydrogel evolution reaction (HER) at the zinc anode accelerates the H_2 generation.[40] When an electric field is applied, the competition between zinc deposition and HER leads to non-uniform electric field distribution and uneven zinc deposition. This results in the formation of dendrites at the anode.[31] In the case of our zwitterionic hydrogel polymer electrolytes, the hydrophilic groups of zwitterions interact with water molecules, and the anionic groups ($-SO_3^-$) interact with zinc cations. These interactions suppress water activation and inhibit water-induced parasitic reactions. Furthermore, through interactions with zinc ions, these zwitterionic hydrogels ensure a uniform distribution of zinc ions. This property could help

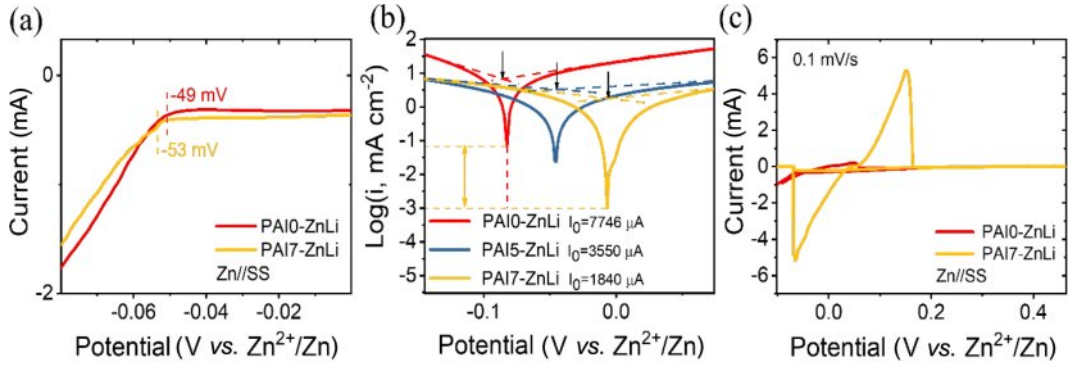

Figure 6. (a) LSV measurements using Zn|PAI0-ZnLi|stainless steel (SS) and Zn|PAI7-ZnLi|SS cells at a scan rate of 0.1 mV/s and 25 °C; (b) Tafel tests using Swagelok cells at 25 °C, with arrows indicating the corrosion potential (E_{corr}); (c) CV tests in the range of -0.1 V to 0.5 V, with a scan rate of 0.1 mV/s and at 25 °C, using Zn|SS cells.

address issues related to desolvation and deposition barriers,[42-44] ultimately reducing such problems and enabling high-density, uniform zinc deposition. To verify this, linear sweep voltammetry (LSV), Tafel, and CV tests were carried out (Figure 6). The HER of the electrolytes was assessed through the LSV curves (Figure 6a). In comparison to the PAI0-ZnLi electrolyte, the PAI7-ZnLi electrolyte exhibited a more negative HER potential (-53 mV).[31,45-47] This indicates that the incorporation of zwitterion (IPS) effectively restricts HER by optimizing the solvation structure between Zn^{2+} cation and zwitterionic chains. The corrosion reaction at the zinc anode was further analyzed using Tafel plots (Figure 6(b)). As the zwitterion content increased from x = 0 to x = 5 and 7 wt%, the corrosion potential (E_{corr}) systematically increased from E_{corr} = -80 mV for PAI0-ZnLi to E_{corr} = -7 mV for PAI7-ZnLi, and the logarithmic corrosion current (i_0) of the zinc electrode became more negative (i_0 = 1840 μA for PAI7-ZnLi), suggesting that corrosion was effectively suppressed by the zwitterion incorporation.[13,14,25,44] To gain further insight into the kinetic behavior of zinc ions, cyclic voltammetry (CV) tests using Zn||SS asymmetric cells were conducted at a scan rate of 0.1 mV/s and 25 ℃ (Figure 6(c)). Unlike PAI0-ZnLi, the PAI7-ZnLi hydrogel polymer electrolyte exhibited a reversible redox reaction, indicating fast zinc plating and stripping processes with a highly current response.[5,43]

The Zn^{2+} transference number was investigated by assembling PAI-ZnLi into Zn||Zn symmetric cells under a constant polarization of 10 mV. In Figure 7(a)-(c), the transference number of zinc ions ($t_{Zn^{2+}}$) was calculated through chronoamperometry and impedance tests using Eq. (2). As the zwitterion content increased, the zinc transference number ($t_{Zn^{2+}}$) increased from 0.49 to 0.7 (Figure 7(d)), indicating that ion migration channels were appropriately formed in the zwitterionic chain due to electrostatic interaction between Zn^{2+} and sulfonic acid groups from VIPS, thus inducing rapid ion transport in the hydrogel.[20,48]

Furthermore, to evaluate the Zn plating/stripping performance, the symmetric Zn||Zn cell was assembled with PAIx-ZnLi (x = 0 and 7 wt%) hydrogel polymer electrolytes having a thickness of 250 μm (Figure 8(a)). In Figure 8(b), the Zn symmetric cell based on PAI7-ZnLi reveals a longer cycle life exceeding 400 hours and a lower overpotential (inset of Figure 8(b)) at a current density of 0.1 mA/cm^2, compared to the PAI0-ZnLi-based cell that exhibited significantly larger overpotential and failed to maintain a steady voltage profile. These results imply that the incorporation of zwitterionic monomer facilitates uniform zinc ion deposition, suppresses Zn dendrite formation, and gives a significant enhancement in the stability of the zinc anode.

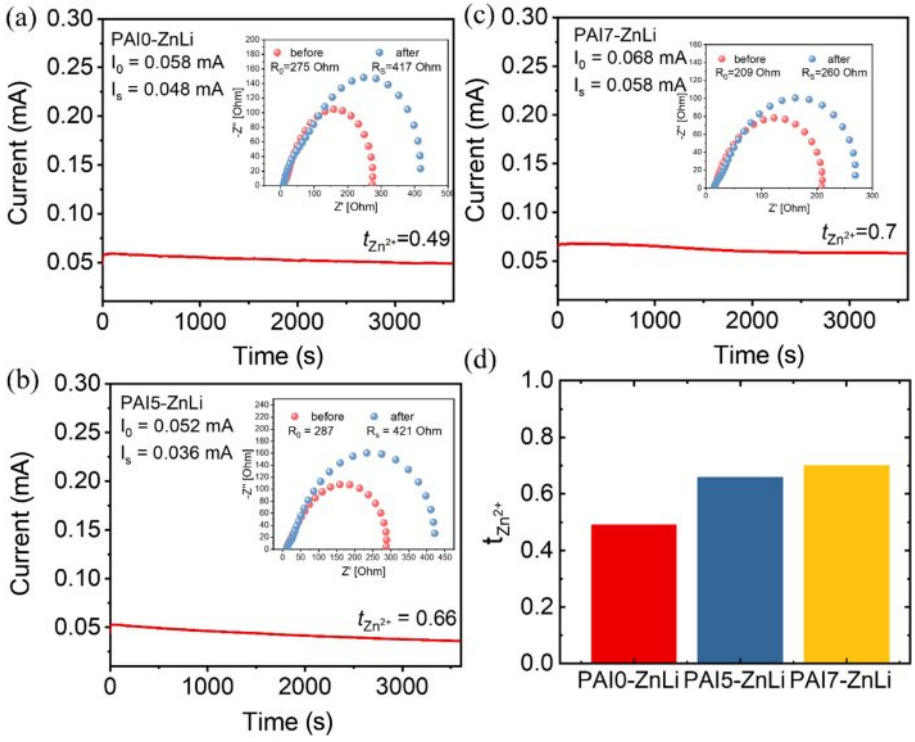

Figure 7. (a-c) Zn^{2+} transference number characterization of (a) PAI0-ZnLi; (b) PAI5-ZnLi; (c) PAI7-ZnLi; (d) comparison of Zn^{2+} transference number of PAI-ZnLi in different amount of VIPS.

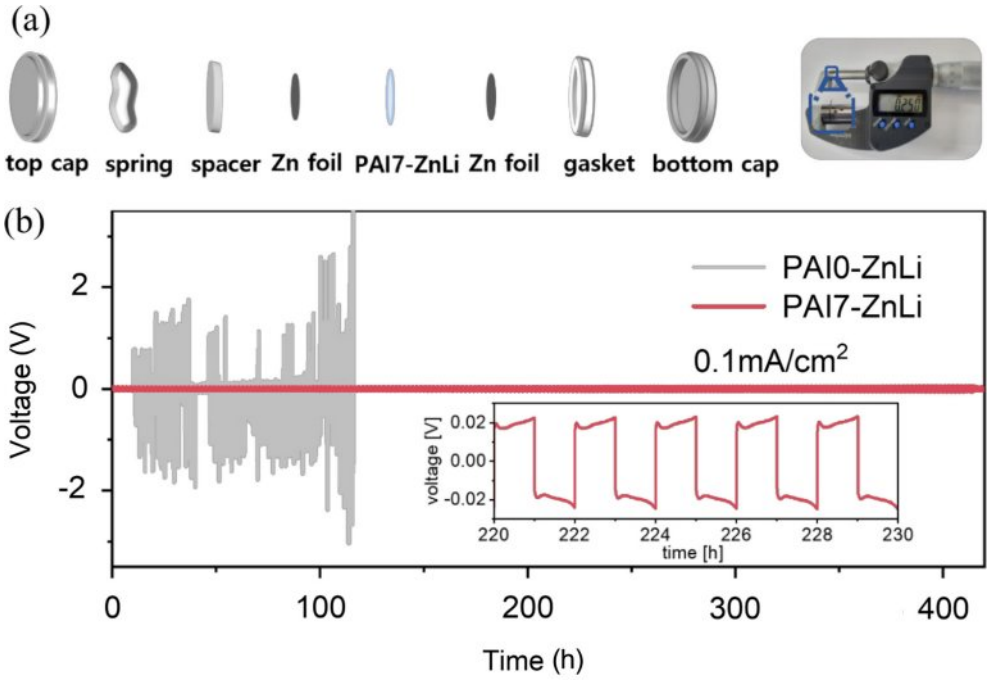

Figure 8. (a) Schematic of coin cell assembly based on Zn||Zn symmetric cell. (b) Zn stripping/plating performance of zinc symmetrical cells with PAI0-ZnLi and PAI7-ZnLi at a current density of 0.1 mA cm^{-2} and inset showing the magnified voltage profile of Zn|PAI7-ZnLi|Zn.

Conclusions

In summary, the zwitterion-based hydrogel polymer electrolytes were successfully synthesized by introducing the cross-linkable acrylamide and zwitterion monomers, along with two different Zn and Li salts. These electrolytes exhibit a stable ionic conductivity even at sub-zero temperatures and demonstrate an impressive 321% stretchability at room temperature. The altered solvation structure resulting from the interaction between zwitterions and zinc cations effectively suppressed both the hydrogen evolution reaction (HER) and corrosion at the zinc electrode. Furthermore, through the fabrication of Zn||Zn cells with our hydrogel polymer electrolyte, the zinc symmetric cell operated stably for over 400 h, confirming the improved safety of our electrolyte with the zinc anode. This result shows the potential of a next-generation aqueous zinc-ion battery.

Acknowledgements: This work was supported by the INHA UNIVERSITY Research Grant.

Conflict of Interest: The authors declare that they have no known competing financial interests or personal relationships that could have appeared to influence the work reported in this paper.

References

1. Iseki, T.; Biutty, M. N.; Park, C. H.; Yoo, S. Il. Local Enhancement of Concentration Gradient Through the Hydrogel-functionalized Anodic Aluminum Oxide Membranes for Osmotic Power Generation. *Macromol. Res.* **2023**, 31, 223-231.
2. So, J.; Kim, T.; Shin, J.; Kim, D.; Kim, F. S. Ionogel-gated Organic Transistors and Artificial Synapses Based on a Composite of Tosylate-doped Poly(3,4-ethylenedioxythiophene) and Insulating Polyvinylpyrrolidone. *Macromol. Res.* **2023**, 31, 1095-1104.
3. Ray, P. K.; Bharati, D. C.; Singh, J. P.; Saroj, A. L. Vibrational, Dielectric and Ion Transport Properties Study of CMC-EDTA-PEG-based Biopolymer Electrolyte Membranes. *Macromol. Res.* **2023**, 31, 539-556.
4. Kim, S. H.; Kim, J. H.; Han, J. H.; Lee, J. Y.; So, S.; Yoon, S. J.; Kim, H.-J.; Lee, K. T.; Kim, T.-H. Cross-Linked Composite Gel Polymer Electrolyte Based on an H-Shaped Poly(ethylene oxide)-Poly(propylene oxide) Tetrablock Copolymer with SiO_2 Nanoparticles for Solid-State Supercapacitor Applications. *ACS Omega* **2021**, 6, 16924-16933.
5. Wang, X.; Wang, B.; Cheng, J. Multi-Healable, Mechanically Durable Double Cross-Linked Polyacrylamide Electrolyte Incorporating Hydrophobic Interactions for Dendrite-Free Flexible Zinc-Ion Batteries. *Adv. Funct. Mater.* **2023**, 33, 2304470.
6. Chen, M.; Chen, J.; Zhou, W.; Han, X.; Yao, Y.; Wong, C.-P. Realizing an All-Round Hydrogel Electrolyte toward Environmentally Adaptive Dendrite-Free Aqueous Zn–MnO_2 Batteries. *Adv. Mater.*

2021, 33, 2007559.
7. Dong, H.; Li, J.; Guo, J.; Lai, F.; Zhao, F.; Jiao, Y.; Brett, D. J. L.; Liu, T.; He, G.; Parkin, I. P. Insights on Flexible Zinc-Ion Batteries from Lab Research to Commercialization. *Adv. Mater.* **2021**, 33, 2077548.
8. Shi, Y.; Wang, R.; Bi, S.; Yang, M.; Liu, L.; Niu, Z. An Anti-Freezing Hydrogel Electrolyte for Flexible Zinc-Ion Batteries Operating at −70 ℃. *Adv. Funct. Mater.* **2023**, 33, 2214546.
9. Zhou, Z.; Wang, H.; Yi, W.; Wu, S.; Sun, X.; Li, J. Engineering of Hydrogel Electrolyte for Aqueous Zn||$LiFePO_4$ Battery on Subzero-temperature Adaptability, Long Cycles and Mechanical Safety. *J. Power Sources* **2023**, 570, 233066.
10. Zhang, Q.; Ma, Y.; Lu, Y.; Zhou, X.; Lin, L.; Li, L.; Yan, Z.; Zhao, Q.; Zhang, K.; Chen, J. Designing Anion-Type Water-Free Zn^{2+} Solvation Structure for Robust Zn Metal Anode. *Angew. Chemie - Int. Ed.* **2021**, 60, 23357-23364.
11. Shin, W.; Chung, K. Correlation Between Solvent Composition and Materials Properties of Organohydrogels Prepared by Solvent Displacement. *Macromol. Res.* **2023**, 31, 615-623.
12. Abdul Kadar, C. H.; Faisal, M.; Maruthi, N.; Raghavendra, N.; Prasanna, B. P.; Manohara, S. R. Corrosion-Resistant Polyaniline-Coated Zinc Tungstate Nanocomposites with Enhanced Electric Properties for Electromagnetic Shielding Applications. *Macromol. Res.* **2022**, 30, 638-649.
13. Huang, S.; He, S.; Li, Y.; Wang, S.; Hou, X. Hydrogen Bond Acceptor Lined Hydrogel Electrolyte Toward Dendrite-Free Aqueous Zn Ion Batteries with Low Temperature Adaptability. *Chem. Eng. J.* **2023**, 464, 142607.
14. Fu, Q.; Hao, S.; Zhang, X.; Zhao, H.; Xu, F.; Yang, J. All-round Supramolecular Zwitterionic Hydrogel Electrolytes Enabling Environmentally Adaptive Dendrite-free Aqueous Zinc Ion Capacitors. *Energy Environ. Sci.* **2023**, 16, 1291-1311.
15. Zeng, Y.; Zhang, X.; Meng, Y.; Yu, M.; Yi, J.; Wu, Y.; Lu, X.; Tong, Y. Achieving Ultrahigh Energy Density and Long Durability in a Flexible Rechargeable Quasi-Solid-State Zn–MnO_2 Battery. *Adv. Mater.* **2017**, 29, 1700274.
16. Yoshizawa-Fujita, M.; Ohno, H. Applications of Zwitterions and Zwitterionic Polymers for Li-Ion Batteries. *Chem. Rec.* **2023**, 23, e202200287.
17. Mei, W.; Rothenberger, A. J.; Bostwick J. E.; Rinehart, J. M.; Hickey, R. J.; and Colby, R. H. Zwitterions Raise the Dielectric Constant of Soft Materials. *Phys. Rev. Lett.* **2021**, 127, 228001.
18. Hladysh, S.; Dvořáková, J.; Proks, V. Synthesis and Anti-fouling Properties of Zwitterionic Poly(l-glutamic acid). *Macromol. Res.* **2023**, 31, 593-601.
19. Zhu, X.; Guo, F.; Ji, C.; Mi, H.; Liu, C.; Qiu, J. Nitrogen-doped Hollow Carbon Nanoboxes in Zwitterionic Polymer Hydrogel Electrolyte for Superior Quasi-solid-state Zinc-ion Hybrid Supercapacitors. *J. Mater. Chem. A* **2022**, 10, 12856-12868.
20. Wu, T.; Ji, C.; Mi, H.; Guo, F.; Guo, G.; Zhang, B.; Wu, M. Construction of Zwitterionic Osmolyte-based Hydrogel Electrolytes Towards Stable Zinc Anode for Durable Aqueous Zinc Ion Storage and Integrated Electronics. *J. Mater. Chem. A* **2022**, 10, 25701-25713.
21. Park, S. M.; Choi, U. H. Highly Stretchable and Conductive Hybrid Gel Polymer Electrolytes Enabled by a Dual Cross-linking Approach. *Macromol. Res.* **2023**, 31, 499-509.
22. Yan, C.; Wang, Y.; Deng, X.; Xu, Y. Cooperative Chloride Hydrogel Electrolytes Enabling Ultralow-Temperature Aqueous Zinc Ion Batteries by the Hofmeister Effect. *Nano-Micro Lett.* **2022**, 14, 98.
23. He, Q.; Fang, G.; Chang, Z.; Zhang, Y.; Zhou, M.; Zhou, M.; Chai, S.; Zhong, Y.; Cao, G.; Liang, S.; and Pan, A. Building Ultra-Stable and Low-Polarization Composite Zn Anode Interface via Hydrated Polyzwitterionic Electrolyte Construction. *Nano-Micro Lett.* **2022**, 14, 93.
24. Yuan, C.; Zhong, X.; Tian, P.; Wang, Z.; Gao, G.; Duan, L.; Wang, C.; Shi, F. Antifreezing Zwitterionic-Based Hydrogel Electrolyte for Aqueous Zn Ion Batteries. *ACS Appl. Energy Mater.* **2022**, 5, 7530-7537.
25. Hao, Y.; Feng, D.; Hou, L.; Li, T.; Jiao, Y.; Wu, P. Gel Electrolyte Constructing Zn (002) Deposition Crystal Plane Toward Highly Stable Zn Anode. *Adv. Sci.* **2022**, 9, 1-10.
26. Handayani, P. L.; Kim, T.; Song, Y. H.; Park, J. S.; Yang, S. J.; Choi, U. H. Tailoring Molecular Interaction in Heteronetwork Polymer Electrolytes for Stretchable, High-voltage Fiber Supercapacitors. *Chem. Eng. J.* **2023**, 452, 139432.
27. Zhu, M.; Wang, X.; Tang, H.; Wang, J.; Hao, Q.; Liu, L.; Li, Y.; Zhang, K.; Schmidt, O. G. Antifreezing Hydrogel with High Zinc Reversibility for Flexible and Durable Aqueous Batteries by Cooperative Hydrated Cations. *Adv. Funct. Mater.* **2020**, 30, 1907218.
28. Zhao, Z.; Liu, Y.; Xian, G.; Wang, Y.; Wu, C.; Peng, X.; Wang, J.; Kong, L. Effect of Compound Coupling Agent Treatment on Mechanical Property and Water Absorption of Hollow Glass Microspheres/epoxy Composite. *Macromol. Res.* **2023**, 31, 771-779.
29. Dhali, K.; Daver, F.; Cass, P.; Adhikari, B. Surface Modification of the Cellulose Nanocrystals Through Vinyl Silane Grafting. *Int. J. Biol. Macromol.* **2022**, 200, 397-408.
30. Chen, Q.; Zhao, J.; Chen, Z.; Jin, Y.; Chen, J. High Voltage and Self-healing Zwitterionic Double-network Hydrogels as Electrolyte for Zinc-ion Hybrid Supercapacitor/battery. *Int. J. Hydrogen Energy* **2022**, 47, 23909-23918.
31. Zhang, W.; Guo, F.; Mi, H.; Wu, Z.-S.; Ji, C.; Yang, C.; Qiu, J. Kinetics-Boosted Effect Enabled by Zwitterionic Hydrogel Electrolyte for Highly Reversible Zinc Anode in Zinc-Ion Hybrid Micro-Supercapacitors. *Adv. Energy Mater.* **2022**, 12, 2202219.
32. Chen, R.; Liu, Q.; Xu, L.; Zuo, X.; Liu, F.; Zhang, J.; Zhou, X.; Mai, L. Zwitterionic Bifunctional Layer for Reversible Zn Anode. *ACS Energy Lett.* **2022**, 7, 1719-1727.
33. Peng, X.; Liu, H.; Yin, Q.; Wu, J.; Chen, P.; Zhang, G.; Liu, G.; Wu, C.; Xie, Y. A Zwitterionic Gel Electrolyte for Efficient Solid-state Supercapacitors. *Nat. Commun.* **2016**, 7, 11782.
34. Fan, Z.; Xu, W.; Wang, R.; Wu, H.; Liu, A. Fast-response Thermo-sensitive Actuator Based on Asymmetric Structured PNIPAM Hydrogel with Inorganic Particles Embedding. *Macromol. Res.* **2023**, 31, 625-633.

35. Yang, W.; Du, X.; Zhao, J.; Chen, Z.; Li, J.; Xia, J.; Zhang, Y.; Cui, Z.; Kong, Q.; Zhao, Z.; Wang, C.; Zhang, Q.; Cui, G. Hydrated Eutectic Electrolytes with Ligand-Oriented Solvation Shells for Long-Cycling Zinc-Organic Batteries. *Joule* **2020**, 4, 1557-1574.
36. Jeong, Y. G.; Park, S. Y.; Kim, J. S.; Lee, Y. Relationship Between the Chemical Structure, Morphology, and Water Absorption of Styrene-co-itaconate Ionomers. *Macromol. Res.* **2023**, 31, 245-255.
37. Li, W.; Xue, F.; Cheng, R. States of Water in Partially Swollen Poly(vinyl alcohol) Hydrogels. *Polymer (Guildf).* **2005**, 46, 12026-12031.
38. Park, S. M.; Choi, U. H. Exceptionally Flexible and Stable Quasi-solid-state Supercapacitors *via* Salt-in-polyampholytes Electrolyte with Non-freezable Properties. *Chem. Eng. J.* **2023**, 479, 147384.
39. Zhang, Z.; Raffa, P. Anti-freezing Conductive Zwitterionic Composite Hydrogels for Stable Multifunctional Sensors. *Eur. Polym. J.* **2023**, 199, 112484.
40. Bayaguud, A.; Fu, Y.; Zhu, C. Interfacial Parasitic Reactions of Zinc Anodes in Zinc Ion Batteries: Underestimated Corrosion and Hydrogen Evolution Reactions and Their Suppression Strategies. *J. Energy Chem.* **2022**, 64, 246-262.
41. Zhu, Y.; Yin, J.; Zheng, X.; Emwas, A-H.; Lei, Y.; Mohammed, O. F.; Cui, Y.; and Alshareef, H. N. Concentrated Dual-cation Electrolyte Strategy for Aqueous Zinc-ion Batteries. *Energy Environ. Sci.* **2021**, 14, 4463-4473.
42. Yu, H.; Chen, D.; Ni, X.; Qing, P.; Wei, W.; Ma, J.; Ji, X.; Chen, Y.; Chen, L. Reversible Adsorption with Oriented Arrangement of a Zwitterionic Additive Stabilizes Electrodes for Ultralong-life Zn-ion Batteries. *Energy Environ. Sci.* **2023**, 16, 2684-2695.
43. Wei, J.; Zhang, P.; Shen, T.; Liu, Y.; Dai, T.; Tie, Z.; and Jin, Z. Supramolecule-Based Excluded-Volume Electrolytes and Conjugated Sulfonamide Cathodes for High-Voltage and Long-Cycling Aqueous Zinc-Ion Batteries. *ACS Energy Lett.* **2023**, 8, 762-771.
44. Zhang, X.; Su, L.; Lu, F.; Tian, Y.; Xie, F.; Liang, L.; Zheng, L.; Gao, X. Tailoring the Hydrophobicity and Zincophilicity of Poly(ionic liquid) Solid-electrolyte Interphases for Ultra-stable Aqueous Zinc Batteries. *Green Chem.* **2023**, 25, 8759-8769.
45. Ciurduc, D. E.; Cruz, C. de la.; Patil, N.; Mavrandonakis, A.; Marcilla, R. Molecular Crowding Bi-salt Electrolyte for Aqueous Zinc Hybrid Batteries. *Energy Storage Mater.* **2022**, 53, 532-543.
46. Wei, T.; Ren, Y.; Li, Z.; Zhang, X.; Ji, D.; Hu, L. Bonding Interaction Regulation in Hydrogel Electrolyte Enable Dendrite-free Aqueous Zinc-ion Batteries From -20 to 60℃. *Chem. Eng. J.* **2022**, 434, 134646.
47. Guan, K.; Yang, R.; Zhang, H.; Wang, N.; Wan, H.; Cui, J.; Zhang, J.; Wang, H.; Wang, H. Anti-Corrosion for Reversible Zinc Anode via a Hydrophobic Interface in Aqueous Zinc Batteries. *Adv. Energy Mater.* **2022**, 12, 2103557.
48. Sun, M.; Ji, G.; Li, M.; Zheng, J. A Robust Hydrogel Electrolyte with Ultrahigh Ion Transference Number Derived from Zincophilic "Chain-Gear" Network Structure for Dendrite-Free Aqueous Zinc Ion Battery. *Adv. Funct. Mater.* **2024**, 34, 2402004.